

Contents list available at CBIORE journal website

International Journal of Renewable Energy Development

Journal homepage: https://ijred.cbiore.id



Research Article

New energy output prediction and demand response optimization based on LSTM-BN

Weisheng Wang¹, Wenhui Shi¹, Dongliang Nan², Yinzhang Peng², Qinghua Wang³, Yankai Zhu³

Abstract. The study proposed a new energy output prediction model based on long and short-term memory network (LSTM)-Bayesian network (BN) by combining the benefits of BN in uncertainty quantification with the processing power of LSTM network to address the issue of volatility and uncertainty of new energy output. Meanwhile, by introducing a price-based demand response mechanism, users were incentivized to increase electricity consumption when the new energy generation was in excess and reduce electricity consumption during the peak period, so as to realize the flexible regulation of loads and the efficient utilization of new energy. The new energy output prediction model developed in the study had the highest degree of match between the anticipated and actual values in various data sets, as demonstrated by the experimental findings, which were above 0.99. In the Google Earth Engin and GEFCom2014 datasets, the operation solution speed was quick and stabilized after 64 and 80 iterations, respectively. Additionally, the model's predicted and actual curve values almost matched, and the actual new energy output power predication's largest prediction error was less than 1%. The implementation of a price-based demand response approach to control customers' power consumption behavior yielded a net benefit of up to 4.45 million yuan for the customers in the target area, based on the precise prediction of new energy output power. The aforementioned findings demonstrated that the LSTM-BN-based new energy output prediction model is capable of precisely projecting new energy output and efficiently matching supply and demand through a price-based demand response mechanism to increase the rate at which new energy is consumed instantly.

Keywords: New energy, Long and short-term memory network, Bayesian network, Price-based demand response strategy



@ The author(s). Published by CBIORE. This is an open access article under the CC BY-SA license (http://creativecommons.org/licenses/by-sa/4.0/).

Received: 9th Sept 2024. Revised: 15th November 2024. Accepted: 26th November 2024. Available online: 12th Dec 2024

1. Introduction

Since there is a lot of volatility and uncertainty associated with new energy generation, it is crucial to predict new energy output accurately and efficiently to optimize the demand response mechanism. This will help to maintain the power grid's stability and increase the efficiency of energy utilization (Malek & Ichinomiya et al., 2023). An intelligent demand response program was created by Huang et al. to address the unpredictability associated with photovoltaic (PV) power generation in microgrids. The program optimized the manufacturing facility's day-ahead production schedule and the battery storage system's operation strategy in response to the probabilistic projections of time segment electric price and PV power generation. The method's effectiveness in lowering manufacturing production's operational expenses was confirmed by the results (Huang et al., 2021). To achieve optimal scheduling, the framework takes into account the uncertainty associated with energy forecasts and employed mixed integer quadratic programming and stochastic model predictive control approaches. The results proved that the method could effectively manage uncertainty in complex microgrids and

enhance their flexibility and economic efficiency in the energy market (Garcia-Torres et al., 2021). Li et al. presented a Chance Constrained Programming-based dispatch model community-based integrated energy systems that includes integrated demand response. The integrated demand response procedure minimized the system operating cost by exploring the potential interaction capability between electric-gas-heat flexible loads and electric vehicles. It can be known that by integrating the demand response procedure, the system is able to manage the demand side resources more efficiently (Li et al., 2021). To achieve intelligent load management and energy allocation strategies, a team of scholars led by Priolkar and Sreeraj proposed a method combining the K-Medoids algorithm and the elephant swarm optimization algorithm. Using this strategy, a price-based demand response program was implemented, and consumers were grouped according to their load consumption habits. The findings indicated that the approach can reduce energy costs and balancing grid loads (Priolkar et al., 2024).

According to the studies of domestic and foreign scholars on new energy grids, the supply side of power generators and the

Email: wangqhcr@126.com (W.Wang)

¹Renewable Energy Res Ctr, China Electric Power Research Institute, Beijing 100192, China

²State Grid Xinjiang Electric Power Science Research Institute, Wulumuqi 830063, China

³School of Energy and Power Engineering, North China Electric Power University, Beijing 100096, China

^{*}Corresponding author

demand side of users are unable to promptly modify their power consumption strategies due to the fluctuations and uncertainties in new energy output, which results in a significant waste of energy. Traditional methods such as time series analysis and regression analysis have limitations in dealing with nonlinear and long-term dependence problems. Long and short-term memory network (LSTM), as a unique type of recurrent neural network (RNN), effectively addresses the long-term dependence problem by introducing mechanisms such as memory units, input gates, forgetting gates, as well as output gates, and shows great potential in new energy output prediction. Bilgili et al. used LSTM network to forecast shortterm energy consumption. The results indicated that the LSTM model had a root mean squared error value of 80.14 GWh and a mean absolute percentage error value of 4.47%. It showed that the short-term daily electric energy consumption using LSTM method time series could provide highly accurate results (Bilgili et al., 2022). A power load forecasting technique based on bidirectional LSTM networks and empirical modal decomposition was presented by Gundu et al. for power consumption data that non-stationary and non-linear characteristics. The results indicated that the method overcome the limitations of traditional forecasting methods in dealing with nonlinear and non-stationary time series data, and could provide strong support for decision making in power supply companies (Gundu et al., 2021).

Meanwhile, as a black-box function optimization technique that gradually approaches the ideal solution by examining and taking advantage of the outcomes of earlier parameter selections, the Bayesian optimization process is widely used in model parameter tuning. To deal with the uncertainty in PV prediction, Abedinia and Bagheri proposed a new synthetic prediction method based on Bayesian network (BN) model

averaging and integrated learning. The method first initializes the training process by utilizing enhanced self-organizing mapping clustering K-fold cross-validation. The outcomes attested that the strategy can significantly raise the accuracy and reliability of PV prediction (Abediniaet al., 2022). Huang et al. introduced a landslide susceptibility prediction model based on incremental learning bayesian network (ILBN). The model improved the accuracy and timeliness of landslide susceptibility prediction by considering continuously updated landslide data. Regarding the current status and shortcomings of the above research, the study proposed a new energy output prediction and demand response optimization method based on LSTM-BN. By constructing the LSTM-BN prediction model, the new energy output can be predicted with high accuracy. In addition to helping users make sensible adjustments to their electricity consumption patterns, it also increases the power grid's capacity to accept new energy sources and preserve operational stability when paired with demand response mechanism optimization.

The study mainly consists of three sections. The first section constructs a new energy generation prediction model based on LSTM-BN, and then uses this prediction result as an input to further construct an optimization model for price and demand response, to improve the utilization efficiency of new energy. The second section mainly describes the dataset and operation environment used for model training, and verifies the performance of the model. The third section mainly summarizes the experimental results in section two and describes the shortcomings of the research method. The study innovatively combines the advantages of LSTM and BN to construct a new energy output prediction model. Meanwhile, a price-based demand response mechanism is introduced to realize the

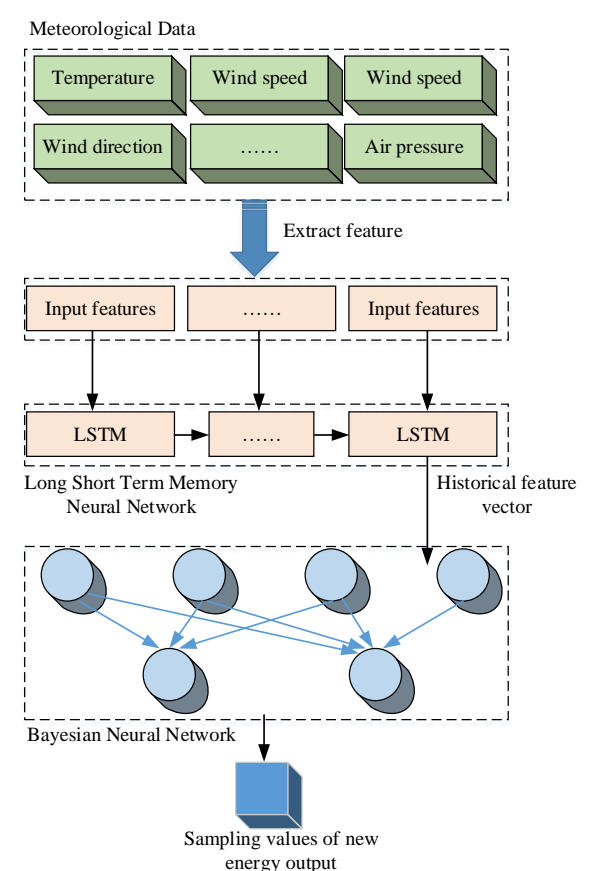


Fig. 1 Steps for new energy output forecasts

flexible regulation of load and the efficient utilization of new energy.

2. Methods and Materials

2.1 New energy output prediction model construction based on LSTM-BN

To enhance the prediction performance of new energy output probability distribution, the study proposes a prediction method based on LSTM and BN. The study takes the prediction of PV output of a random user in a typical day as the object, and the new energy output prediction step of LSTM-BN constructed is shown in Figure 1.

In Figure 1, accurately prediction the output of wind farms and PV power plants over a given time period in the future is the primary objective of new energy prediction. The steps for predicting the output of new energy are divided into four steps. First is to collect meteorological information near PV power plants and wind farms, including temperature and the speed and direction of the wind. The second step uses pass path analysis to examine the meteorological information of new energy base on the correlation of meteorological factors and derive the characteristics of meteorological information. The third step uses LSTM to extract the time-series characteristics of new energy output on a typical day in history. In the fourth step, a BN-based prediction model is constructed, and the meteorological and time-series features are used as inputs to obtain the probability distribution of the output of new energy. Then, sampling is performed according to the probability distribution to generate multiple possible forecast values.

For the analysis and screening of new energy meteorological characteristics, firstly, the meteorological factor information required for Q new energy is collected in the user's T-side period, setting the q type of meteorological information as x_q , the class q meteorological information at the t moment as x_{qt} , and the solar power output data as y_t . The correlation $C_{x_q \to y_t}$ between x_q and y_t is calculated as shown in Eq. (1) (Huang et q_t , 2022).

$$C_{x_{qt} \to y_t} = \frac{\sum_{t=1}^{T} (x_{qt} - \bar{x}_q)(y_t - \bar{y}_t)}{\sum_{t=1}^{T} (x_{qt} - \bar{x}_q)^2} \sqrt{\frac{\sum_{t=1}^{T} (x_{qt} - \bar{x}_q)}{\sum_{t=1}^{T} (y_t - \bar{y}_t)}}$$
(1)

The correlation coefficients $C_{x_q \to x_p \to y_t}$ of type q meteorological information x_q with PV output data after the influence of type p meteorological x_p information are shown in Eq. (2).

$$C_{x_q \to x_p \to y_t} = \frac{\sum_{t=1}^{T} (x_{qt} - \bar{x}_q)(x_{pt} - \bar{x}_p)}{\sqrt{\sum_{t=1}^{T} (x_{qt} - \bar{x}_q)^2 \sum_{t=1}^{T} (x_{pt} - \bar{x}_p)^2}} C_{x_p \to y_t}$$
(2)

Solar irradiance, illumination duration, temperature, humidity, and other variables are among the data chosen for new energy PV (Dong *et al.*, 2022). Wind direction, wind intensity, temperature, humidity, and other factors are among the data chosen for new energy wind farms (Dhiman *et al.*, 2021). The correlation between new energy PV output and meteorological information in the study area is analyzed using Eq. (1) and Eq. (2). A total of z groups of meteorological information are selected to form the meteorological feature vectors required by the model $X_t^{wea} = (x_{1t}, x_{2t}, ..., x_{nt})$

The temporal features of the meteorological information of the study area are then extracted using the construction of the LSTM, setting the model to have L network units, and at moment t, the output of the a LSTM network unit is predicted to be X_{at}^{in} , as shown in Eq. (3) (Liu et al., 2022).

$$X_t^{wea} = concat(X_{1t}, Y_{2t}) (3$$

In Eq. (3), X_t is the meteorological information feature vector, y_t is the PV outflow data, X_{at}^{in} is the splicing of the previous two, and $concat(\cdot)$ is the splicing operation. The minimum cell structure of LSTM is shown in Figure 2 (Kumar *et al.*, 2021).

In Figure 2, C_t , C_{t-1} , C_{t-2} , h_t , h_{t-1} , and h_{t-2} are the status of each learning units, i_t is the input gate, as shown is Eq. (4) (Ma *et al.*, 2021).

$$i_t = \delta \left[\left[W_i(h_t), X_{at}^{in} \right] + b_i \right] \tag{4}$$

In Eq. (4), δ is the activation function, b_i is the bias constant, W_i is the weight matrix of the input gates, and f_i is the forgetting gate, as denoted in Eq. (5).

$$f_t = \delta \left[\left[W_f(h_t), X_{at}^{in} \right] + b_f \right] \tag{5}$$

In Eq. (5), W_f is the weight matrix of the forgetting gate and o_t is the output gate, as denoted in Eq. (6).

$$o_t = \delta \left[\left[W_o(h_t), X_{at}^{in} \right] + b_o \right] \tag{6}$$

In Eq. (6), W_o in z is the weight matrix of the output gate. The learnable unit states C_t and h_t are shown in Eq. (7).

$$\begin{cases}
C_t = f_t C_t + i_t \tanh[W_c[h_t, X_t^{in}] + b_c] \\
h_t = o_t \tanh(C_t)
\end{cases}$$
(7)

In Eq. (7), h_t is the state of the learnable unit, W_c is the weight matrix of the learnable unit. The LSTM network unit captures the long-term dependencies in the time series through the gating mechanism to realize the extraction of new energy weather information features, see Figure 3 (Liu *et al.*, 2021) (Kong *et al.*, 2021).

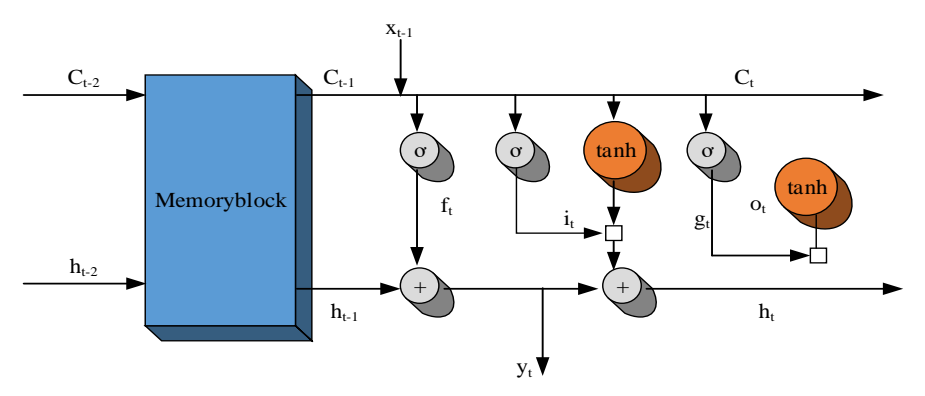


Fig. 2. LSTM minimum cell structure

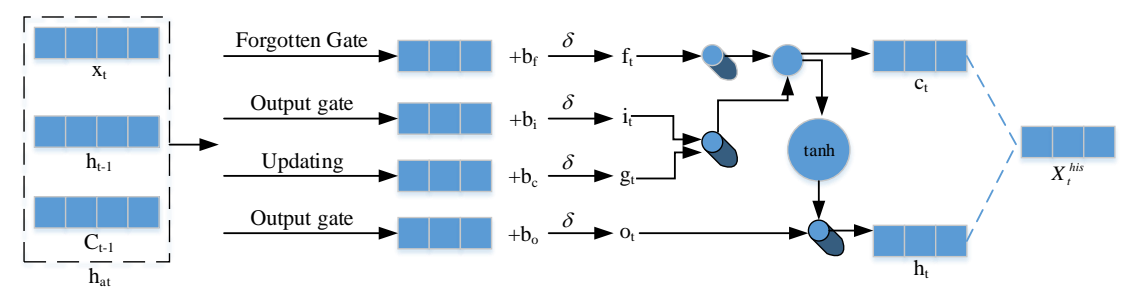


Fig. 3. New energy weather time series feature vector extraction process

As shown in Figure 3, the unit state of the a LSTM network unit is set to h_{at} . The new energy weather timing feature vector X_t^{his} is output after the LSTM network.

Then the BN is constructed to predict the new energy output, and the meteorological information feature vector X_t^{wea} of the study area at the moment of t and the new energy meteorological time-series feature vector X_t^{his} output after the LSTM network are spliced as the input feature vector $X_t^b = concat(X_t^{wea}, X_t^{his})$ of the BN, which is used as the basis for the prediction of new energy output value. The prior distribution of the BN constructed by the study is Gaussian distribution, as denoted in Eq. (8) (Sharma *et al.*, 2021) (Fortuin *et al.*, 2022).

$$p(W) = \prod_{j=1}^{N_w} \pi N(w_j; 0, \gamma_{01}^2) + (1 - \pi) N(w_j; 0, \gamma_{02}^2)$$
 (8)

In Eq. (8), W is the probability layer parameter of the BN, π is the mixing proportion of the Gaussian distribution, w_j is the j parameter of the probability layer of the BN, γ_{01}^2 and γ_{02}^2 are the variances under the normal distribution, and N_w is the total number of parameters of the probability layer of the network. In the BN prediction model, the input feature splicing vector is X, the output new energy output prediction is Y, and the a posteriori probability of the BN is p(W/X,Y). The approximate distribution $q(W;\vartheta)$ of the new energy output prediction is introduced, which is shown in Eq. (9) (Jia *et al.*, 2020) (Moe *et al.*, 2021).

$$q(W;\vartheta) = \prod_{j=n}^{N_w} N(w_j; \mu_j; \delta_j^2)$$
 (9)

In Eq. (9), ϑ is the learned parameter of the model, μ_j is the mean value of the j parameter, and δ_j^2 is the parameter variance. The a sampling value of the j parameter in the model is calculated according to the approximate distribution, as shown in Eq. (10) (Feng $et\ al.$, 2021).

$$w_i^a = \mu_i + \log(1 + e^{p_i}) \otimes z^{is} \tag{10}$$

In Eq. (10), \otimes is the Hadamard product and z^{is} is the multidimensional distribution of meteorological information in the normal distribution. Based on Eq. (10), the a sampling parameter $W_j^A = \left(w_1^a, w_2^a, \ldots, w_{N_w}^a\right)$ in the BN network model (Hebbi $et\ al.$, 2023) is obtained. The new energy outflow prediction Y of the output can be obtained by taking the feature splicing vector X as input in the BN network model and propagating it forward in the model, see Eq. (11).

$$Y = f(X_t; W_i^A) \tag{11}$$

2.2 Optimization model construction for user-side price demand response

A appropriate demand response strategy can be developed to balance the power supply and demand relationship once the new energy output has been effectively predicted(Xia *et al.*, 2021). By optimizing the demand response strategy, the power

system's uncertainty about the new energy output can also be decreased (Sharma *et al.*, 2022). Figure 4 depicts the processes of the customer-side price demand response optimization model

As illustrated in Figure 4, the study is based on the forecast data of new energy output, and then the price demand response optimization model is established with the aim of minimizing the total cost of user energy overhead. Electricity user demand response optimization strategies can mainly split into price-type and incentive-type. The study adopts the price-based demand response optimization strategy, which guides users to adjust their energy use behavior through the signal of electricity price changes to achieve power optimization (Mokayed *et al.*, 2023). The power load transfer in the customer-side price demand response optimization model is shown in Eq. (12).

$$p^l = p^0 + \Delta p \tag{12}$$

The user load matrices p^l and p^0 in Eq. (12) are the user load matrices following and prior to the price-demand ring optimization model adoption, respectively. Δp denotes the user load transfer matrix, and Δp is shown in Eq. (13).

$$\Delta p = E \bullet \Delta[p] \oplus p^0 \tag{13}$$

In Eq. (13), E is the matrix of elasticity coefficients of users for multiple time periods. $\Delta[p]$ is the normalized matrix of the rate of change of the indicated time-of-day tariffs. These two matrices are calculated in Eq. (14) (Huang *et al.*, 2023).

$$\begin{cases}
\Delta[p] = \left[\frac{\Delta p_2}{p_1^0}, \frac{\Delta p_2}{p_2^0}, \dots, \frac{\Delta p_T}{p_T^0}\right]^T \\
E = \begin{bmatrix}
e_{11} & e_{12} & \dots & e_{1T} \\
e_{21} & e_{22} & \dots & e_{2T} \\
\dots & \dots & \dots & \dots \\
e_{T1} & e_{T2} & \dots & e_{TT}
\end{bmatrix}
\end{cases} (14)$$

In Eq. (14), Δp_T is the difference between the tariff used by the customer at moment T and the benchmark tariff, p_T^0 is the benchmark tariff of the electricity used by the customer at moment T, and e_{TT} is the auto-elasticity coefficient of row T, column T in the matrix of the multi-temporal elasticity coefficients of the customer. For the target study area, users of different load types (electricity, heat, and gas) each enjoy different forms of output from new energy sources. The electric load users integrate their own PV generation and share the electricity from the regional wind power, the thermal load users receive the thermal part of the energy converted by the wind power, and the gas load users are allocated the gas energy converted by the wind power (Iweh et al., 2021). For each time t(s = 1,2,...T), within each season s(s = 1,2,...S), the new energy output of these three load types for user i is calculated as shown in Eq. (15).

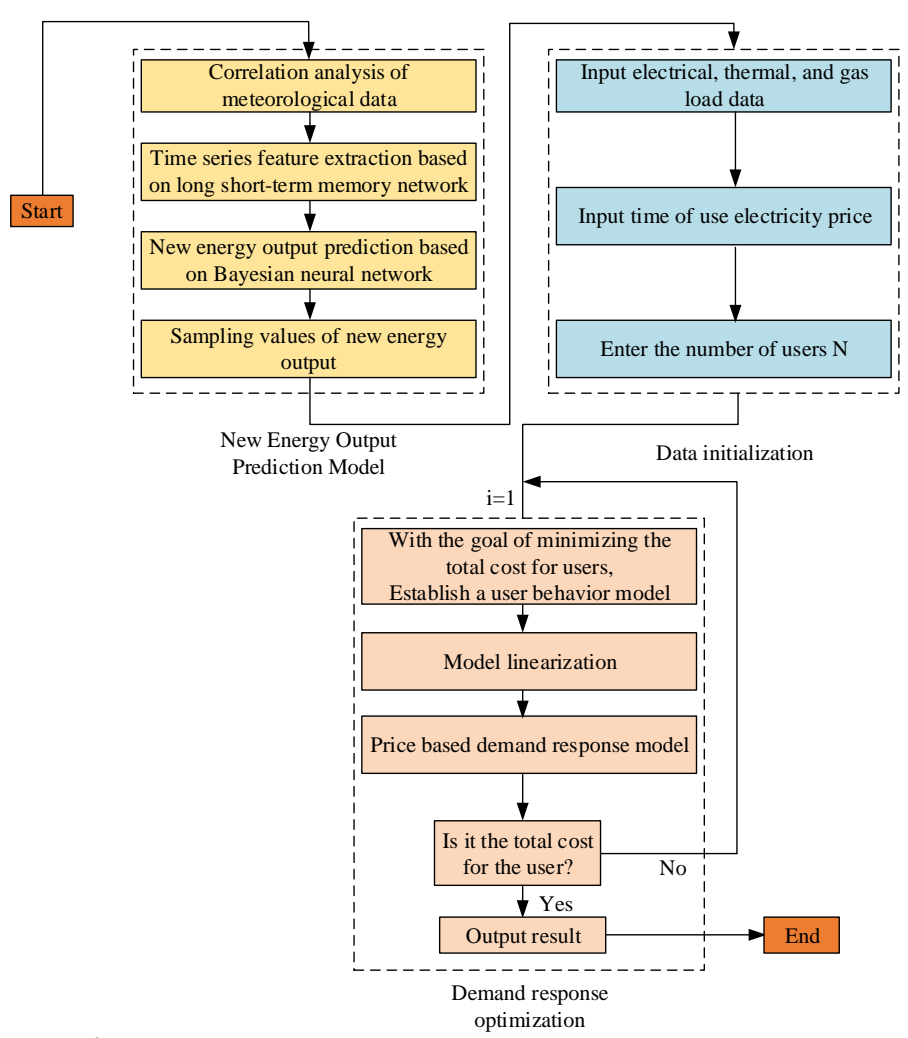


Fig. 4. Steps for running the user-side price demand response optimization model

$$\begin{cases} p_{s,t,i}^{e,NE} = p_{s,t,i}^{PV} + w p_{s,t,i}^{WP} \\ p_{s,t,i}^{h,NE} = v (1 - w) p_{s,t,i}^{WP} \eta^{P2G} \eta^{GB} \\ p_{s,t,i}^{g,NE} = (1 - v) (1 - w) p_{s,t,i}^{WP} \eta^{P2G} \end{cases}$$
(15)

In Eq. (15), s is the meteorological season, t is the time, i is the user, $p_{s,t,i}^{e,NE}$ is the t time to provide electrical load of new energy output, $p_{s,t,i}^{PV}$ is the t time of its own PV power generation, $p_{s,t,i}^{WP}$ is the t time of wind power in the apportionment of the power, w is the apportionment coefficient, $p_{s,t,i}^{h,NE}$ is the t time to provide thermal load of new energy output, v is the apportionment coefficient, $p_{s,t,i}^{g,NE}$ is the t time to provide gas load of new energy output. The function of the sharing coefficient is to allocate the total output of new energy to different types of loads, and its calculation method differs based on the system, which may be ascertained using empirical formulas (Baik et al., 2022). Meanwhile, the new energy output has uncertainties, and the need for energy storage and loading when there is a surplus of energy, also, the need for external energy supplementation when there is a shortage of energy (Song et al., 2023). Therefore, the study introduces a multienergy cloud energy storage model for users, which makes use of the big data and real-time information in the cloud platform to formulate and optimize the charging and discharging strategies. The cloud energy storage user meets its load demand by leasing the right to use the energy storage from the cloud energy storage provider, thus avoiding the fixed cost of directly purchasing and operating and maintaining physical energy storage equipment (Su et al., 2024). The total cost to the subscriber consists of two components: firstly, the leasing service fee to the equipment service as the initial investment cost of using the cloud energy storage technology, and secondly, the operational overheads borne by the additional energy procurement from the electricity, heat and natural gas networks required to safeguard the operation in the face of power shortages or cloud energy storage resource constraints (Zhang & Lyu et al., 2021). According to different user selection methods, it can be divided into three scenarios. In scenario one, electricity, heat, and gas users operate independently, each with their own energy storage system. These energy storage systems are used to balance the uncertainty of new energy output, ensuring that sufficient energy can be provided when new energy output is insufficient, and excess energy can be stored when new energy output is surplus. Users can independently decide how to use energy based on their own energy needs and the status of the energy storage system. In scenario two, the users give up building their own energy storage system and instead purchases cloud energy storage services. Cloud energy storage service providers are responsible for the construction and operation of energy storage systems, and users only need to pay rental and usage fees. Users decide how to use energy based on the status of cloud energy storage services and their own energy needs. When cloud energy storage resources are limited or energy is insufficient, users need to purchase additional energy from electricity, heat, and natural gas

networks. In scenario three, users further introduce a demand response optimization model on the basis of purchasing cloud energy storage services. This model guides users to adjust their energy consumption behavior through electricity price change signals, achieving electricity optimization. Users use demand response optimization models to adjust energy usage based on electricity price change signals and their own energy needs. For example, increasing energy use when electricity prices are low, reducing energy use or transferring loads when electricity prices are high. To maximize economic benefits, the user aims to minimize their equivalent annual cost, accounting for the cost of leasing cloud storage services and the additional cost of purchasing energy from other energy networks (natural gas, heat, and electricity) due to energy shortages or limited cloud storage resources, as indicated in Eq. (16).

$$\begin{cases} \min C_{1} = k_{pa}C_{inv,i} + C_{2} \\ k_{pa} = \frac{r(1+r)^{d}}{(1+r)^{d}-1} \\ \frac{\max_{2e,j} \max_{e,j} \max_{e,j} \max_{e,j} \max_{e,j} \max_{e,j} \max_{e,j} \sum_{e,j} \max_{e,j} \max_{e,$$

In Eq. (16), k_{pa} is the equal annual value coefficient, C_1 is equivalent annual value cost, d is the length of time the energy storage device is used, r is the annual interest rate, C_2 is the operating cost of the user using the cloud energy storage, $C_{inv,i}$ is the investment cost, kf_1 and kf_2 are the lithium battery's service charge per unit of power and per unit of capacity, respectively, $p_{f,i}^{max}$ and $e_{f,i}^{max}$ are the maximum power provided by the cloud energy storage and the maximum limit value of the cloud gas storage capacity, respectively, kg_1 and kg_2 are the energy conversion rate of the heat storage tank and the capacity cost, respectively, kv_1 and kv_2 are the energy conversion rate and capacity cost of the gas storage tank, respectively. Because the cost minimization model contains segmented functions, it is difficult to solve it conventionally. Therefore, the nonlinear constraints containing segmented functions are linearized using the "Big M method", which is mainly realized by introducing auxiliary variables and 0-1 variables. It is assumed that one of the segmented functions in the solution function is f(x), see Eq. (17) (Jayaprakash et al., 2023) (Cao et al., 2024).

$$f(x) = \begin{cases} \max\{x, 0\} \\ \min\{x, 0\} \end{cases}$$
 (17)

To represent f(x), an auxiliary variable y is introduced such that y = max(x, 0). The 0-1 variable is then used to indicate the sign of x. Assuming that the 0-1 variable is u, the representation is shown in Eq. (18).

$$\begin{cases} y \leq x + M(1 - u_1) \\ y \leq M(1 - u_2) \\ u_1 + u_2 \geq 1 \\ u_1, u_2 \in \{0, 1\} \end{cases}$$
 (18)

In Eq. (18), M is a large constant. u_1 and u_2 are both 0-1 variables. Finally, all these constraints are integrated into the new energy user cost minimization solving problem. The original problem is converted to a mixed integer linear programming (MILP) problem, which is then solved using a standard MILP solver to solve the user-minimized annual value cost, and the new energy output demand response optimization can be realized. It is capable of achieving the optimization of new energy output demand response.

To demonstrate the prediction accuracy of the LSTM-BN model constructed in the study, three evaluation indexes, namely, normalized root mean square error (NRMSE), correlation coefficient between predicted and real values (R^2),

and average percentage error (APE) are selected to quantitatively evaluate the prediction ability of the model. NRMSE is a significant statistic for determining the difference between projected and actual values, with a smaller value indicating a more accurate prediction. The calculation method is displayed in Eq. (19) (Viktor *et al.*, 2023).

$$NRMSE = \sqrt{\frac{\sum (y_{\text{true}} - y_{\text{pred}})^2}{\sum (y_{\text{true}} - y_{\text{mean}})^2}}$$
 (19)

In Eq. (19), y_{true} , y_{pred} , y_{mean} stand for the mean of the true value, predicted value, and true value, respectively. APE directly reflects the percentage of prediction error to the actual value, and a lower APE value denotes a more accurate prediction. The calculation method is as denoted in Eq. (20) (Irfan *et al.*, 2021).

$$APE = \sqrt{\frac{y_{\text{actual}} \cdot y_{\text{pred}}}{y_{\text{actual}}} \times 100\%}$$
 (20)

In Eq. (20), y_{actual} and y_{pred} stand for the mean of the true value, predicted value, respectively. The R^2 value is used to quantify the degree of correlation between the predicted values and the actual observed values of the model. The calculation method is in Eq. (21) (Long *et al.*, 2023).

$$R^2 = 1 - (\sum (y_{\text{true}} - y_{\text{pred}})^2) / (\sum (y_{\text{true}} - y_{\text{mean}})^2)$$
 (21)

The model's predictive power increases with the R^2 value's proximity to 1.

3. Result and Discussion

3.1 Performance analysis and application testing of new energy output prediction models

To validate the effectiveness of the new energy output prediction model constructed in the study with the LSTM-BN, the Google Earth Engin dataset and GEFCom2014 dataset were selected as the training data for the model. The Google Earth Engin dataset is an open and unified spatial dataset for wind and solar installations, which records the location, capacity, and historical output data of wind and solar installations in a certain region. The GEFCom2014 dataset contains multiple dimensions of data, including actual and predicted values of new energy loads in a certain region, fluctuations in electricity prices, realtime data on wind power, and predicted and actual output of solar power generation. The study first preprocessed two datasets, performing tasks like data cleansing, addressing missing values, and detecting and processing outliers, to ensure data quality and consistency when using the Google Earth Engin dataset and GEFCom2014 dataset for the detection and validation of new energy output prediction models (Borrohou et al., 2023). Next, it was divided into a training set and a testing set in a 4:1 ratio. The training set is used for model training, and the testing set is used to evaluate the predictive performance of the model. The operating environment and parameter settings of the model are displayed in Table 1.

The fitting degree of the predicted and actual values of the LSTM-BN model was first determined in the two datasets respectively, and to illustrate the superiority of the research methodology, the BN model, the SEAM-LSTM model, and the CL-LSTM model were selected to form a control experiment with the research-constructed model under the same experimental conditions. The results are shown in Figure 5.

In Figure 5, the predicted values of the LSTM-BN model constructed in the study fitted the real values to the highest degree, and the SEAM-LSTM model also has a higher degree of fit, but there is still a gap with the LSTM-BN model, which

 Table 1

 Running environment and parameterization of the model

Project	Parameter			
System	Window 10			
GPU	NVIDIA Tesla H800			
CPU	AMD Ryzen 9 7950X3D			
Memory	DDR5 6400 32GB(16GBx2			
Development language	Python			
Hidden layer output unit	25			
Initial learning rate	0.005			
Iterations	160			
Number of hidden layers	3			
Optimizer	Adam			
loss function	Cross-Entropy			
Epoch number	50			
Review window size	600×600			

Table 2

Comparative results of the predictive power of the four models

Method	Google Earth Engin dataset			GEFCom2014 dataset		
	NRMSE	R ²	APE	NRMSE	R ²	APE
LSTM-BN	0.0088	0.9965	0.432	0.0075	0.9987	0.332
SEAM-LSTM	0.0123	0.9901	0.521	0.0232	0.9712	0.421
CL-LSTM	0.0235	0.8636	0.765	0.0325	0.8652	0.655
BN	0.0560	0.8421	0.865	0.0456	0.8465	0.745

reflects the effectiveness of the present model in dealing with the long term temporal dependence of the data. Comparing the results in Figures 5(a), (b), (e) and (f), as shown, the LSTM-BN model has the potential to greatly increase the prediction accuracy by capturing the features of meteorological information through the LSTM and then optimizing the prediction of new energy power generation using the BN technique. When the LSTM is missing in the LSTM-BN model, the deviation of the prediction results becomes larger and the prediction accuracy is reduced. Comparing the results in Figures 5(a) and (e), it can be obtained that the predicted values of the LSTM-BN model constructed by the study fitted well with the true values both in the GEFCom2014 dataset and in the Google Earth Engin dataset, which indicates that the model has some generalization, and it can produce better prediction

results in various usage scenarios. The NRMSE, R^2 , and APE statistical results of the four algorithms are shown in Table 2.

Table 2 shows the detailed results of the predictions of the four models in two kinds of data, and it can be found that the LSTM-BN model constructed by the study has the highest R² value and the lowest NRMSE and APE values, whether it is tested in the GEFCom2014 dataset or in the Google Earth Engin dataset. This indicates that the model constructed in the study can predict the new energy power output data more accurately.

This is because the LSTM structure in the research and construction model is adept at handling long-term dependencies in time series data, and can effectively capture the temporal characteristics of new energy output. BN updates the posterior distribution of model parameters by combining prior knowledge and observation data, which helps improve the generalization ability and prediction accuracy of the model.

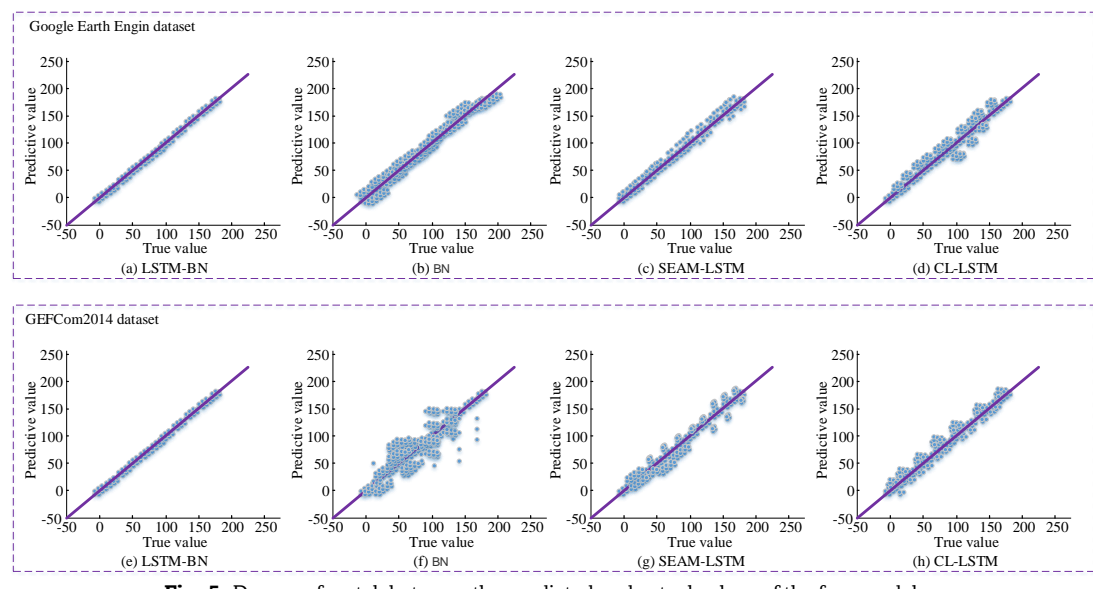


Fig. 5. Degree of match between the predicted and actual values of the four models

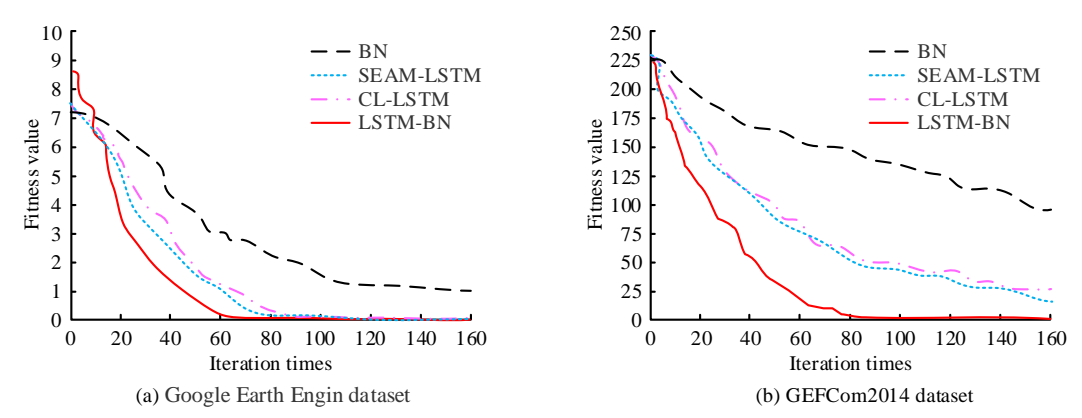


Fig. 6. Computational speed of the four models

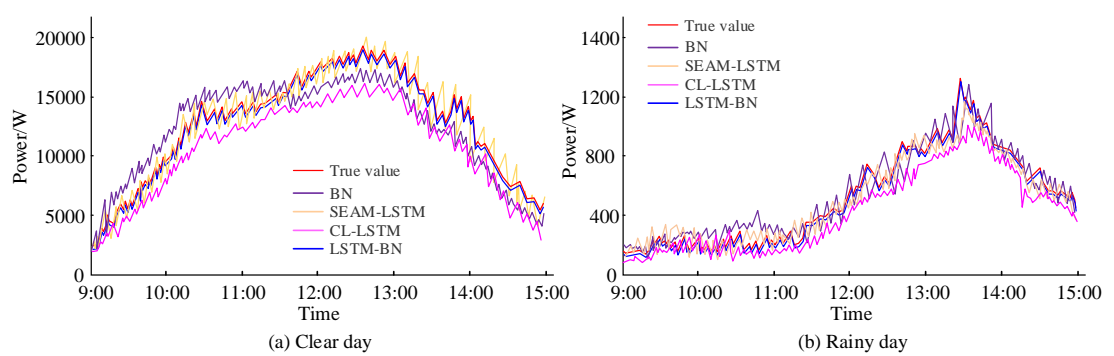


Fig. 7. Prediction results of new energy output power by four models

Although SEAM-LSTM and CL-LSTM also adopt the LSTM structure, their predictive performance is slightly inferior to the LSTM-BN model due to insufficient optimization of model parameters. The standalone BN model cannot fully capture the temporal features in the data, resulting in poor predictive performance. Then the prediction speeds of the four models are tested, and the results are shown in Figure 6.

From Figure 6(a), in the Google Earth Engin dataset, the LSTM-BN model demonstrated excellent performance. It only needs about 64 iterations, and its fitness value quickly reaches a stable state, indicating that the model can efficiently capture data features and optimize the model. In contrast, the SEAM-LSTM model requires 80 iterations to stabilize its fitness value, while the CL-LSTM model requires 82 iterations. Although the convergence speed of these two models is slightly slower than that of the LSTM-BN model, they still demonstrated some optimization ability when processing this dataset. However, the BN model faced significant optimization difficulties when processing this dataset, requiring 112 iterations to stabilize the

fitness value, and its stable fitness value was higher than the first three models. In the GEFCOm2014 dataset, the LSTM-BN model also demonstrated efficient computational capability and excellent generalization ability. After about 82 iterations, the fitness value tended to stabilize. This further validates the stability and optimization efficiency of the LSTM-BN model on different datasets. However, SEAM-LSTM, CL-LSTM, and BN models performed poorly in this dataset. Their fitness values did not reached a stable state at the end of training, indicating that these models may face optimization difficulties and relatively weak generalization ability when processing certain datasets. The LSTM-BN model demonstrated excellent generalization ability in two different datasets. Its fitness value could quickly reach a stable state and maintain stable optimization effects in different data environments. This indicated that the LSTM-BN model had strong data adaptability and robustness, making it the preferred model for tasks such as time series prediction. In contrast, SEAM-LSTM, CL-LSTM, and BN models showed weaker generalization ability.

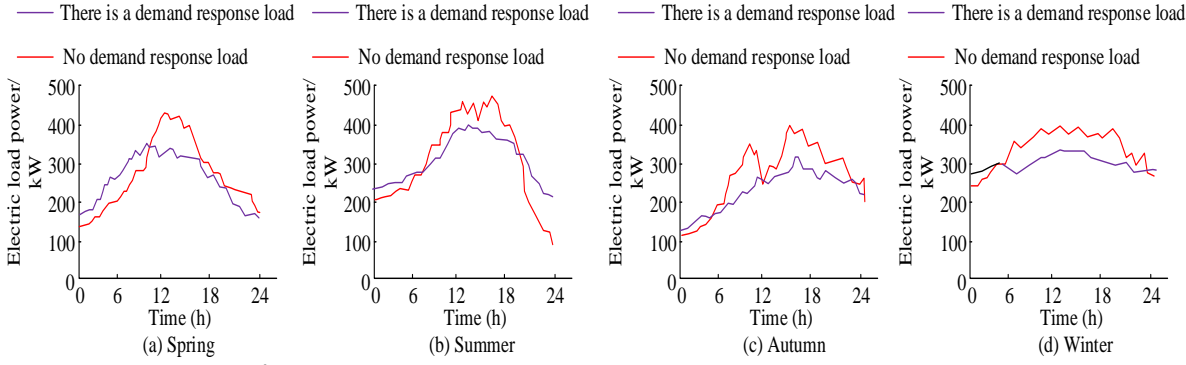


Fig. 8. Comparison of Before and After Adopting Demand Response Programs

The model was trained on data from January to December 2023 from distributed new energy generation systems deployed on the rooftop of an industrial park, and the data sampling interval was set at once every minute to eliminate abnormal and invalid information. Finally, 12,568 high-quality data points are retained for subsequent research. At the same time, numerical weather forecast data from neighboring weather stations were introduced for training, and the trained model was utilized to forecast the new energy output power on a random day, and the results are shown in Figure 7.

From Figure 7, it is evident that the new energy power system had a maximum output power of 18865W on sunny days, and it is concentrated between 11:00-14:00. And the highest power output power in rainy days was only 1356W, which was concentrated between 13:00-14:00. In terms of the overall prediction, the curve value between the predicted one and the true one of the LSTM-BN model constructed in the study almost overlapped, and the maximum prediction error does not exceed 1%. In contrast, the prediction curves of the SEAM-LSTM model, CL-LSTM model and BN model had relatively large errors with the true curves, and could not accurately predict the output power of the new energy power system.

3.2 Analysis of user-side price demand response optimization results

Once the new energy output power in the target area is accurately predicted using the LSTM-BN model, the corresponding demand response optimization strategy can be formulated based on the prediction results. The study set each season as a 91-day cycle, and for typical days, a 24-hour dispatch cycle was determined. Due to the characteristics of the cloud energy storage system that does not require frequent immediate response, the dispatch interval of the system was set to be 1 hour to optimize the energy allocation. In addition, the time-of-day tariff mechanism of a neighborhood was used, which was specifically divided into three time periods, namely, peak time, usual time, and valley time, and the impact of tariff changes on the scheduling strategy was simulated based on the specific tariff and time period divisions. The comparison of electricity load in a neighborhood after citing the demand response design methodology designed by the study is shown in Figure 8.

In Figure 8, the peak period of electricity consumption in this neighborhood in either season was around 12:00-21:00 and the low period is from 0:00-6:00 every day. Before the study's demand response plan was implemented, there was a lot of variation in the load profiles of the customers' electricity usage. In contrast, the load volume curves began to flatten out regardless of the season after the study's optimum scenario was added. The charge increases during the low peak period of power use and fell during the peak period. Next three comparison scenarios were set up to compare the impact of demand response and time-of-use tariff strategies. Scenario 1: Electricity, heat, and gas users are independent, their own energy storage systems are built, and a new energy output prediction model is used. Scenario 2: Users abandon their own energy storage and purchase cloud energy storage services. Scenario 3: Based on Scenario 2, a demand response optimization model is added, i.e., users adjust their energy use base on the price of electricity and their own needs. The comparison of one day's electricity load for the three scenarios is shown in Figure 9.

As shown in Figure 9, Scenario 2 exhibited a more significant peak shaving effect due to the configuration of the energy storage system. In contrast, the model of Scenario 3 not only reduced energy storage system's operating costs but also better improved the fluctuation of the load curve by optimizing the

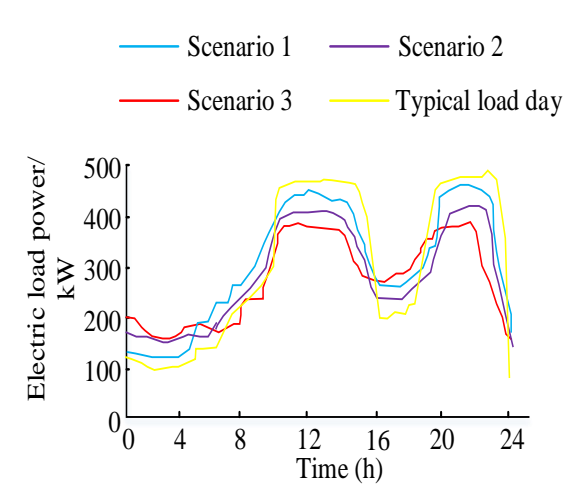


Fig. 9. Comparison of power load in different scenarios

energy storage capacity configuration and time-sharing tariff strategy, resulting in a smoother load curve. The results of the fixed investment cost and the whole life cycle net benefit of the users under the three scenarios are shown in Figure 10.

In Figure 10(a), the fixed investment costs for users in Scenarios 1, 2 and 3 are \$2.78 million, \$3.52 million and \$3.52 million, respectively. This is due to the fact that the users of Scenarios II and III need to purchase the cloud storage power system as well as bear its maintenance costs. As shown in Figure 10(b), the whole life cycle net benefits for users of Scenarios 1, 2 and 3 are \$2.15 million, \$3.54 million, and \$4.45 million, respectively. This indicated that the user's use of the cloud energy storage system reduces the overall operating cost and improves the energy use efficiency, thus increasing the net benefit. The use of a demand response optimization model considerably increases the net benefit. After optimization, users are able to better adapt to fluctuations in electricity prices and achieve more efficient energy use and greater economic returns.

4. Conclusion

Facing the strong uncertainty of new energy output, the study put forward a new energy output prediction method based on LSTM-BN. The approach used the BN for power forecasting after extracting the new energy weather quantity vector features using the LSTM network. It gave future energy system planning a strong data foundation. Next, considering the important influence of price-based demand response in the market mechanism on user behavior, a user-side demand response model was established. Users were guided to adjust their electricity consumption behavior through price signals. The LSTM-BN constructed in the study outperformed other algorithms both in prediction accuracy and budget speed. Regarding prediction accuracy, the NRMSE value of LSTM-BN model was less than 0.0090, R^2 was more than 0.99, and APE was less than 0.5. In budget speed, the LSTM-BN model tended to stabilize with 64 iterations and 80 iterations in the Google Earth Engin and GEFCom2014 datasets, respectively, with the lowest value of the fitness. After the LSTM-BN model accurately predicted the new energy output, a price-based demand response strategy was introduced. The results indicated that the demand response method used in the study flattened the load curve and had an important role in peak shaving and valley filling. Meanwhile, after applying the demand response optimization model, the whole life cycle net benefit of the users in the region was maximized, which was 4.45 million RMB. It showed that the LSTM-BN model had very high prediction

accuracy and fast convergence speed in new energy output prediction, which gave great support for the power system's stability and efficiency. However, different users have geographic variability and potential volatility, and subsequent research will focus on modeling and analyzing user behavioral non-volatility to improve the applicability of the model.

Fundings

The research is supported by: State Grid Corporation of China Headquarters Technology Project (No. 5100-202255354A-2-0-YS).

Reference

- Abedinia, O., Bagheri, M. (2022). Execution of synthetic Bayesian model average for solar energy forecasting. *IET Renewable Power Generation*, 16(6), 1134-1147.https://doi.org/10.1049/rpg2.12389
- Baik, S. H., Yoon, Y. T., & Jin, Young GyuMoon, HeeSeungKim, Seung Wan. (2022). Managing power imbalance with cloud energy storage in imbalance band market environment. *IET generation, transmission & distribution*, 16(17), 3522-3538. https://doi.org/10.1049/gtd2.12542
- Bilgili, M., Arslan, N., ŞEKERTEKİN, A., YAŞAR, A. (2022). Application of long short-term memory (LSTM) neural network based on deeplearning for electricity energy consumption forecasting. *Turkish Journal of Electrical Engineering and Computer Sciences*, 30(1), 140-157.https://doi.org/10.3906/elk-2011-14
- Borrohou, S., Fissoune, R., & Badir, H. (2023). Data cleaning survey and challenges–improving outlier detection algorithm in machine learning. *Journal of Smart Cities and Society*, 2(3), 125-140. https://doi.org/10.3233/SCS-230008
- Cao, D. X., Zhou, X. X., Guo, X. Y., & Song, N. (2024). Limit cycle oscillation and dynamical scenarios in piecewise-smooth nonlinear systems with two-sided constraints. *Nonlinear Dynamics*, 112(12), 9887-9914. https://doi.org/10.1007/s11071-024-09589-6
- Dong, T., Yin, S., & Zhang, N. (2022). New energy-driven construction industry: Digital green innovation investment project selection of photovoltaic building materials enterprises using an integrated fuzzy decision approach. Systems, 11(1): 11. https://doi.org/10.3390/systems11010011
- Dhiman, H. S., Deb, D., Muyeen, S. M., & Kamwa, I. (2021). Wind turbine gearbox anomaly detection based on adaptive threshold and twin support vector machines. *IEEE Transactions on Energy Conversion*, 36(4), 3462-3469. https://doi.org/10.1109/TEC.2021.3075897
- Feng, R., Balling, N., Grana, D., Dramsch, J.S., Hansen, T.M. (2021). Bayesian convolutional neural networks for seismic facies classification. *IEEE Transactions on Geoscience and Remote Sensing*, 59(10), 8933-8940. https://doi.org/10.1109/TGRS.2020.3049012
- Garcia-Torres, F., Bordons, C., Tobajas, J., Real-Calvo, R., Santiago, I., Grieu, S. (2021). Stochastic optimization of microgrids with hybrid energy storage systems for grid flexibility services considering energy forecast uncertainties. *IEEE Transactions on Power Systems*, 36(6), 5537-5547.https://doi.org/10.1109/TPWRS.2021.3071867
- Gundu, V., Simon, S.P. (2021). PSO-LSTM for short term forecast of heterogeneous time series electricity price signals. *Journal of Ambient Intelligence and Humanized Computing*, 2021, 12(2), 2375-2385.https://doi.org/10.1007/s12652-020-02353-9
- Fortuin, V. (2022). Priors in bayesian deep learning: A review. *International Statistical Review*, 90(3), 563-591. https://doi.org/10.48550/arXiv.2105.06868
- Hebbi, C., Mamatha, H. (2023). Comprehensive dataset building and recognition of isolated handwritten Kannada characters using machine learning models. *Artificial Intelligence and Applications*, 1(3), 179-190. https://doi.org/10.47852/bonviewAIA3202624
- Huang, C., Zhang, H., Song, Y., Wang, L., Luo, X. (2021). Demand response for industrial micro-grid considering photovoltaic power uncertainty and battery operational cost. IEEE Transactions on Smart Grid, 12(4), 3043-3055.https://doi.org/10.1016/j.ijepes.2018.10.006
- Huang, F., Ye, Z., Zhou, X., Huang, J., Zhou, C. (2022). Landslide susceptibility prediction using an DER adoption forecast for distribution grid planning using bayesian bass diffusion model incremental learning Bayesian Network model considering the

- continuously updated landslide inventories. *Bulletin of Engineering Geology and the Environment*, 81(6), 1-19. https://doi.org/10.1007/s10064-022-02748-2
- Huang, L., Qin, J., Zhou, Y., Zhu, F., Liu, L., & Shao, L. (2023). Normalization techniques in training dnns: Methodology, analysis and application. *IEEE transactions on pattern analysis and machine* intelligence, 45(8), 10173-10196. https://doi.org/10.1109/TPAMI.2023.3250241
- Ichinomiya, H., Kawabe, K., Chaitusaney, S. (2023). DER adoption forecast for distribution grid planning using bayesian bass diffusion model. *Journal of Japan Society of Energy and Resources*, 44(3), 135-144. https://doi.org/10.1016/j.ijepes.2018.10.006
- Irfan, Faisal M Avub. N Althobiani Zain Ali Muhammad Idrees Saeed Ullah Saifur Rahman AbdAlwadieSaleh ullah Saeed Mohammed GhonaimHeshamAbdushkourFahad Salem AlkahtaniSamarAlqhtaniPiotr Gas. (2022). Energy theft identification using adaboostensembler in the smart grids. Computers, materials & 2141-2158. 72(3). https://doi.org/10.32604/cmc.2022.025466
- Iweh, C. D., Gyamfi, S., Tanyi, E., &Effah-Donyina, E. (2021). Distributed generation and renewable energy integration into the grid: Prerequisites, push factors, practical options, issues and merits. *Energies*, 14(17), 5375-5376. https://doi.org/10.3390/en14175375
- Jayaprakash, K. R., Tandel, V., &Starosvetsky, Y. (2023). Dynamics of excited piecewise linear oscillators. *Nonlinear dynamics*, 111(6), 5513-5532. https://doi.org/10.1007/s11071-022-08108-9
- Jia, X., Yang, J., Liu, R., Wang, X., Cotofana, S.D., Zhao, W. (2020). Efficient computation reduction in bayesian neural networks through feature decomposition and memorization. *IEEE Transactions on Neural Networks and Learning Systems*, 32(4): 1703-1712. https://doi.org/10.1109/TNNLS.2020.2987760
- Kong, F., Li, J., Jiang, B., Wang, H., & Song, H. (2021). Integrated generative model for industrial anomaly detection via bidirectional LSTM and attention mechanism. *IEEE Transactions on Industrial Informatics*, 19(1), 541-550. https://doi.org/10.1109/TII.2021.3078192
- Kumar, S., Damaraju, A., Kumar, A., Kumari, S., Chen, C.M. (2021).
 LSTM network for transportation mode detection. *Journal of Internet Technology*, 22(4), 891-902.https://doi.org/10.53106/160792642021072204016
- Li, Y., Wang, B., Yang, Z., Li, J., Li, G. (2021). Optimal scheduling of integrated demand response-enabled community-integrated energy systems in uncertain environments. *IEEE Transactions on Industry Applications*, 58(2), 2640-2651.https://doi.org/10.1109/TIA.2021.3106573
- Liu, C., Zhang, Y., Sun, J., Cui, Z., Wang, K. (2022). Stacked bidirectional LSTM RNN to evaluate the remaining useful life of supercapacitor. *International Journal of Energy Research*, 46(3), 3034-3043.https://doi.org/10.1002/er.7360
- Liu, Q., Long, L., Peng, H., Wang, J., Yang, Q., Song, X., & Pérez-Jiménez, M. J. (2021). Gated spiking neural P systems for time series forecasting. *IEEE Transactions on Neural Networks and Learning Systems*, 34(9), 6227-6236. https://doi.org/10.1109/TNNLS.2021.3134792
- Long, B., & Jiang, Z. (2023). Estimation and prediction for two-parameter pareto distribution based on progressively double type-ii hybrid censored data. aims mathematics, 8(7), 15332-15351. https://doi.org/10.3934/math.2023784
- Lyu, J., Zhang, S., Cheng, H., Yuan, K., Song, Y., Fang, S. (2021). Optimal sizing of energy station in the multienergy system integrated with data center. *IEEE Transactions on Industry Applications*, 57(2), 1222-1234.https://doi.org/10.1109/TIA.2021.3054607
- Ma, C., Lin, C., Samuel, O.W., Guo, W., Zhang, H. (2021). Greenwald S A bi-directional LSTM network for estimating continuous upper limb movement from surface electromyography. *IEEE Robotics and Automation Letters*, 6(4), 7217-7224.https://doi.org/10.1109/LRA.2021.3097272
- Malek, S.N.H., Jemat, A. (2023). Consumer concerns on smart meter usage in Malaysia. *Acta Informatica Malaysia (AIM)*, 7(1), 15-18. https://doi.org/10.26480/aim.01.2023.15.18
- Moe, S. J., Wolf, R., Xie, L., Landis, W. G., Kotamäki, N., & Tollefsen, K. E. (2021). Quantification of an adverse outcome pathway network by Bayesian regression and Bayesian network modeling. *Integrated*

- Environmental Assessment and Management, 17(1), 147-164. https://doi.org/10.1002/ieam.4348
- Mokayed, H., Quan, T.Z., Alkhaled, L., Sivakumar, V. Real-time human detection and counting system using deep learning computer vision techniques. *Artificial Intelligence and Applications*, 1(4), 221-229. https://doi.org/10.47852/bonviewaia2202391
- Priolkar, J., Sreeraj, E.S. (2024). Analysis of price based demand response program using load clustering approach. *IETE Journal of Research*, 70(2), 2091-2104. https://doi.org/10.1080/03772063.2022.2161956
- Sharma, H., Jennings, E. (2021). Bayesian neural networks at scale: a performance analysis and pruning study. *Journal of Supercomputing*, 77(4), 3811-3839. https://doi.org/10.1007/s11227-020-03401-z
- Sharma, P., Said, Z., Kumar, A., Nizetic, S., Pandey, A., Hoang, A. T., & Tran, V. D. (2022). Recent advances in machine learning research for nanofluid-based heat transfer in renewable energy system. Energy & Fuels, 36(13), 6626-6658. https://doi.org/10.1021/acs.energyfuels.2c01006
- Song, H., Lu, X., Zhang, X., Tang, X., & Zhang, Q. (2023). Collaborative optimization for energy saving and service composition in multigranularity heavy-duty equipment cloud manufacturing

- environment. Journal of Industrial and Management Optimization, 19(4), 2742-2771. https://doi.org/10.3934/jimo.2022063.
- Su, Y. J., & Yang, S. Y. (2024). A user-friendly cloud-based multi-agent information system for smart energy-saving. *Journal of Internet Technology*, 25(2), 293-300. https://doi.org/10.1186/s13677-024-00615-x.
- Viktor, Szabó., Katarzyna Osińska-Skotak., & Olszak, T., (2024). Using machine learning techniquesto reconstruct the signal observed by the grace mission based on amsr-e microwave data. *Miscellanea Geographica*, 28(2), 80-86. https://doi.org/10.2478/mgrsd-2023-0033
- Xia, M., Shao, H., Ma, X., & De Silva, C. W. (2021). A stacked GRU-RNN-based approach for predicting renewable energy and electricity load for smart grid operation. *IEEE Transactions on Industrial Informatics*, 17(10), 7050-7059. https://doi.org/10.1109/TII.2021.3056867
- Zhang, N., Jiang, H., Li, Y., Yong, P., Li, M., Zhu, H., Kang, C. (2021). Aggregating distributed energy storage: Cloud-based flexibility services from China. *IEEE Power and Energy Magazine*, 19(4), 63-73. https://doi.org/10.1109/MPE.2021.3072820



© 2025. The Author(s). This article is an open access article distributed under the terms and conditions of the Creative Commons Attribution-ShareAlike 4.0 (CC BY-SA) International License (http://creativecommons.org/licenses/by-sa/4.0/)